Intrusion of the North Pacific waters into the South China Sea

Tangdong Qu

International Pacific Research Center, SOEST, University of Hawaii, Honolulu

Humio Mitsudera

Frontier Research System for Global Change, Tokyo
International Pacific Research Center, SOEST, University of Hawaii, Honolulu

Toshio Yamagata

Department of Earth and Planetary Physics, University of Tokyo, Tokyo
Frontier Research System for Global Change, Tokyo

Abstract. Water mass distribution was studied by analyzing historical hydrographic data in the South China Sea. Despite considerable modification of characteristics as a result of mixing, waters of both salinity maximum and minimum of the North Pacific origin were traced on the density surfaces around 25.0 and 26.73 σ_θ, respectively. In the salinity maximum layer, property distribution suggests an intrusion into the South China Sea all year-round through the Luzon Strait. The seasonal variation of the intrusion contains a pronounced semiannual signal, with greater strength in winter and summer than in spring and fall. From spring to fall, the intrusion water from the Pacific is narrowly confined in the continental slope south of China; only in winter, when the northeast monsoon becomes fully developed, can it spread in the southern South China Sea. In the salinity minimum layer, water enters the South China Sea only in spring, when the intrusion in the salinity maximum layer is weakest. A combined use of the "island rule" with climatological data suggests a mean Luzon Strait transport of the order 4 Sv (1 Sv = 10^6 m^3 s^{-1}).

1. Introduction

It has been known for several decades that there is an intrusion of waters from the Pacific into the South China Sea through the Luzon Strait. Since the Luzon Strait is the only deep (>2500 m) passage of the South China Sea (Figure 1), the intrusion is important both to the heat and to the salt budgets of the basin. *Wyrtki* [1961] provided the first estimate of the intrusion and demonstrated that waters enter the South China Sea in winter and flow back to the Pacific in summer in response to the seasonally reversing monsoon. Recent observations [e.g., *Shaw*, 1989] found further evidence that the intrusion of the Pacific waters toward the region southwest of Taiwan occurs even in summer, when the prevailing wind is from the southwest.

More recently, *Shaw* [1991] prepared a climatic picture of the intrusion, based on historic hydrographic data in the northern South China Sea. According to his results, the Kuroshio front meanders into the Luzon strait from June to September, but there is little indication of a westward flow farther west during that period of time. As northeast monsoon develops in late fall and winter, waters of the North Pacific origin flow hundreds of kilometers westward along the continental margin south of China and have a notable impact on the water characteristics of the entire northern South China Sea. The intrusion decays during the transition season of monsoon from February to May. Shaw's analysis may be representative in a sense of statistics, because of the combined use of data from various cruises in different years. However, it considered only the statistical aspects of waters around the salinity maximum

layer in the northern South China Sea. Little is known in the deeper layers and in the southern part of the basin. Furthermore, as can be seen in the following sections [see also *Nitani*, 1972], the depth of the salinity maximum in the South China Sea is considerably shallower than in the Philippine Sea. Thus analysis of water masses on pressure surfaces may not be especially appropriate for the region close to the Luzon Strait.

Numerical models have become powerful tools and have shown many interesting results concerning the intrusion in the Luzon Strait. Among them, *Metzger and Hurlburt* [1996] suggest that the intrusion is a year-round phenomenon; that is, water from the Pacific enters the South China Sea during all seasons of the year. However, no direct observational confirmation has been published so far.

Here we utilize all hydrographic data available in the National Oceanographic Data Center (NODC) archives as of the first quarter of 1993. We focus on two well-defined water masses: the high-salinity North Pacific Tropical Water (NPTW) and the low-salinity North Pacific Intermediate Water (NPIW) [cf *Reid*, 1965; *Tsuchiya*, 1968]. At the Philippine coast, most of these waters recirculate to the north via the Kuroshio, with only a small part turning equatorward into the Mindanao Current [e.g., *Lukas et al.*, 1991; *Qu et al.*, 1998]. Because of the intrusion in the Luzon Strait, these North Pacific waters also escape into the South China Sea. The main purpose of this study is to prepare maps of water mass distribution both in the salinity maximum and in the salinity minimum layers over the entire basin of the South China Sea. These maps are then used as a passive tracer to provide direct information on the pathway of the intrusion in the Luzon Strait.
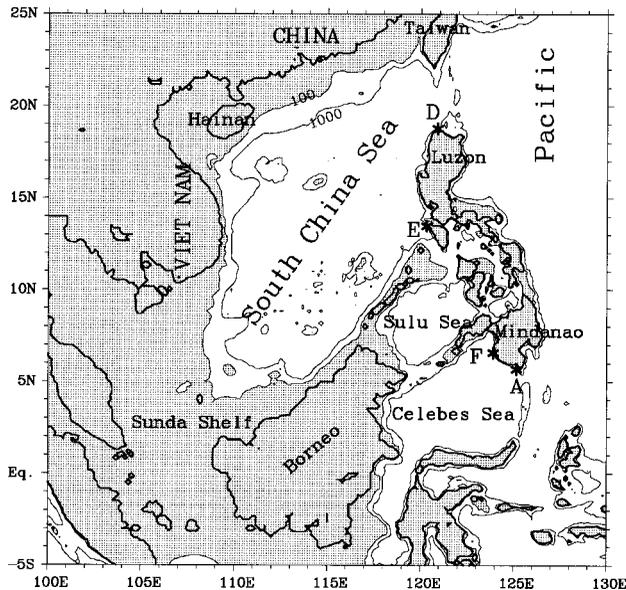
Figure 1. Map of the South China Sea with the 100 and 1000 isobaths shown. Region with water depth shallower than 100 m is stippled.

2. Data and Methods of Analysis

Hydrographic profiles at observed levels recorded on the CD-ROMs of the "World Ocean Atlas 1994" of NOAA/NESDIS/NODC (called the NODC data set below) within the region enclosed by the 100-m isobath in the South China Sea (3°–25°N, 105°–120°E) and in the northern Philippine Sea (15°–25°N, 120°–125°E) are used for this study (Figures 2a–2b). As already noted by many earlier studies, even after extensive editing, some NODC profiles still contain erroneous records both in coordinates and in measured values. The primary procedure for the quality control of data in this study includes removal of profiles with obviously erroneous records and profiles displaying features that do not match the characteristics of surrounding profiles. After such an editing, the data set provide 6800 profiles of temperature-salinity and 1715 profiles of dissolved oxygen concentration in the region studied. The observations of temperature/salinity spanned the period from the 1940s to the early 1990s. The data coverage for the seasonal cycle is generally good, with 1948 samplings in spring, 2021 in summer, 1542 in fall, and 1289 in winter.

Water masses are traced either as salinity extremes or as isopycnal surfaces. Properties are averaged and smoothed in a $0.5° \times 0.5$ grid. Considering that there are few stations in some grid bins, we choose a variable horizontal radius to include at least five observations at each grid. Standard deviations are calculated during the averaging process and used to edit the resulting mean in each grid (see the Appendix). Observations that differed from the grid mean by more than three standard deviations were discarded. The mean property fields are finally smoothed using Gaussian filter with an e-folding scale of about 150 km [*Qu et al.*, 1999].

3. Mean Characteristics

Salinity at observed levels is plotted against potential temperature and dissolved oxygen concentration in Figure 3. Water properties in the northern South China Sea have been documented by several earlier studies [e.g., *Wyrtki*, 1961; *Nitani*, 1972; *Shaw*, 1991]. A prominent feature is that at any given depth in the upper thermocline the Pacific water is warmer and saltier than the South China Sea water. East of the Luzon Strait, most stations have a salinity maximum exceeding 35.0 psu and a homogeneous layer of oxygen concentration (about 4.5 mL L⁻¹). As we progress southwestward, the strength of the salinity maximum becomes weaker, reaching a value of 34.75 psu or less at oxygen level between 3.5 and 4.0 mL L⁻¹ in the southern South China Sea, apparently as a result of mixing in the ocean. This trend is reversed in the salinity minimum layer, where salinity is found to be lowest (<34.25 psu) east of the Luzon Strait and considerably higher to the southwest. Despite weaker extreme properties, waters of both salinity maximum and minimum can be seen in most parts of the South China Sea.

3.1. NPTW

On the basis of Figure 3, a wide density range of 23.5–25.5 σ_θ was chosen in which to search for NPTW. Figure 4a shows the location of stations where at least one salinity maximum is measured in this density range (dots, called the salinity maximum stations below). The probability of salinity maximum, defined as the percentage occurrence of the salinity maximum stations in each grid, shows a decrease toward the south from about 0.8 in the Luzon Strait to about 0.3 on the Sunda Shelf.
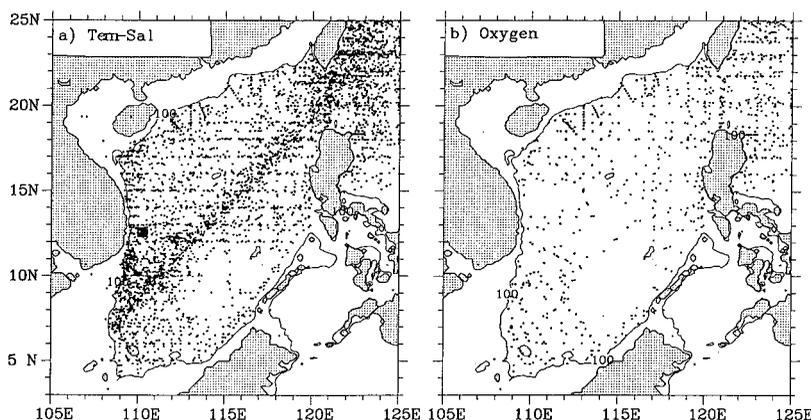

Figure 2. Station distributions of (a) temperature-salinity and (b) oxygen used in this study.

A high-probability belt extending southwestward along the continental slope south of China reflects the strong influence of the North Pacific sources on the water masses in the northern South China Sea. The probability distribution to the south contains a pattern of basically northeast-southwest–oriented contours with a positive gradient toward the northwest.

NPTW in the South China Sea resides roughly on density surfaces around 25.0 σ_θ at depths between 120 and 150 m, with shallower depth and lower density on the northern side (Figures 4b–4c). The density of NPTW is lower than 24.6 σ_θ east of the Luzon Strait and tends to increase southwestward. According to *Qu et al.* [1999] this change of density could be explained as a result of mixing. Considering that temperature usually has more importance than salinity in the state equation, mixing of temperature and salinity in the salinity maximum may not be compensated, thus leading to a change of density in favor of temperature.

Temperature and salinity decrease along the coast south of China and east of Vietnam, giving the typical picture of a tongue-like spreading (Figures 4d–4e). Associated with this high temperature and salinity distribution is elevated concentration of dissolved oxygen (Figure 4f), indicative of a strong link to the Kuroshio where water has a higher oxygen concentration than in the South China Sea. In the southernmost part of the basin the salinity maximum (<34.575 psu) is no longer well pronounced, lying at temperatures of about 17°C and oxygen levels of less than 2.8 mL L^{-1}.

Since water parcels are expected to flow along isopycnal surfaces, we have also included maps of property distribution on 25.0 σ_θ surface that intersects NPTW (Figure 5). The pattern does not differ in any significant ways from that shown in Figures 4d–4e except for a narrower range of potential temperate (17.7° < T < 18.2°C).

3.2. NPIW

NPIW was defined as a salinity minimum in the density range of 26.5–27.0 σ_θ [*Qu et al.*, 1999]. Compared to Figure 4a, the spatial distribution of NPIW is relatively uniform (Figure 6a, dots), with the probability of a salinity minimum higher than 0.7 in a limited region south of China and between 0.5 and 0.6 in most parts of the basin. This result implies that NPIW is probably better conserved and transported for a greater distance than NPTW, presumably because of weak mixing below the seasonal thermocline.

The spreading of NPIW in the South China Sea is narrowly confined on density surfaces around 26.73 σ_θ at depth between 480 and 500 m (Figures 6b–6c). Interestingly, despite strong temperature and salinity gradients in the Luzon Strait (Figures 6d–6e), density of NPIW remains fairly stable. Away from the Luzon Strait, water properties have relatively narrow ranges, at 8.4° < θ < 8.8°C, 34.40 < S < 34.46 psu, and 1.7 < O$_2$ < 2.4 mL L^{-1} (Figures 6d–6f). Water of nearly homogenous temperature (8.6°–8.7°C) and salinity (34.42–34.44 psu) with elevated oxygen level (>2.0 mL L^{-1}) is seen north of the line from about 10°N, 110°E to 15°N, 120°E, consonant with its supply from the North Pacific subtropical gyre. To the south, temperature and salinity slightly increase, exceeding 8.8°C and 34.45 psu, respectively, near the coast of Borneo. Similar phenomena are also seen in maps of property distribution on a density surface of 26.73 σ_θ (Figure 7).

4. Seasonal Variations

The seasonal forcing in the South China Sea is dominated by the northeast monsoon in winter and the southwest monsoon
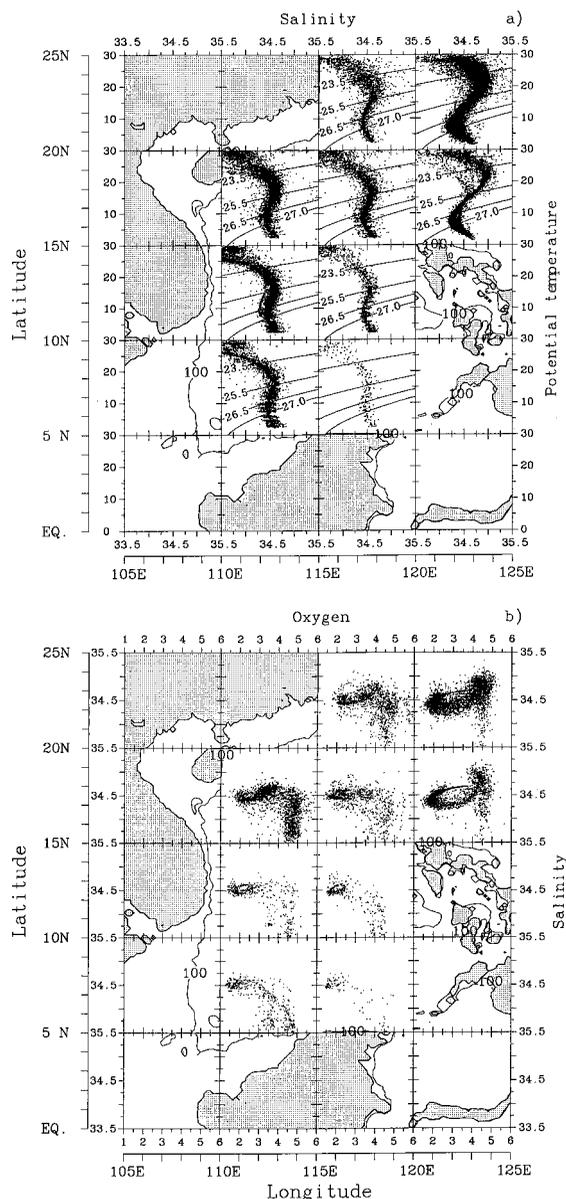

Figure 3. Relations of (a) potential temperature versus salinity and (b) salinity versus oxygen in a grid of 5° × 5°.

in summer. The northeast monsoon first appears in the northern South China Sea in September and then extends over the entire basin from October to February; the southwest monsoon prevailing during the period from mid-May to August is relatively weaker [*Hellerman and Rosenstein*, 1983]. To investigate the response of the intrusion to the seasonally reversing monsoon, distributions of salinity on 25.0 and 26.73 σ_θ surfaces are examined for four periods of the year: March–May, June–August, September–November, and December–February, representing the conditions of monsoon (summer and winter) and transition (spring and fall) seasons, respectively.

4.1. NPTW

The intrusion of waters on 25.0 σ_θ surface shows a significant seasonal signal. In spring (March–May) the salinity distribution contains primarily two patterns (Figure 8a). South of the 34.60 psu isohaline, located roughly from 15°N, 110°E to the
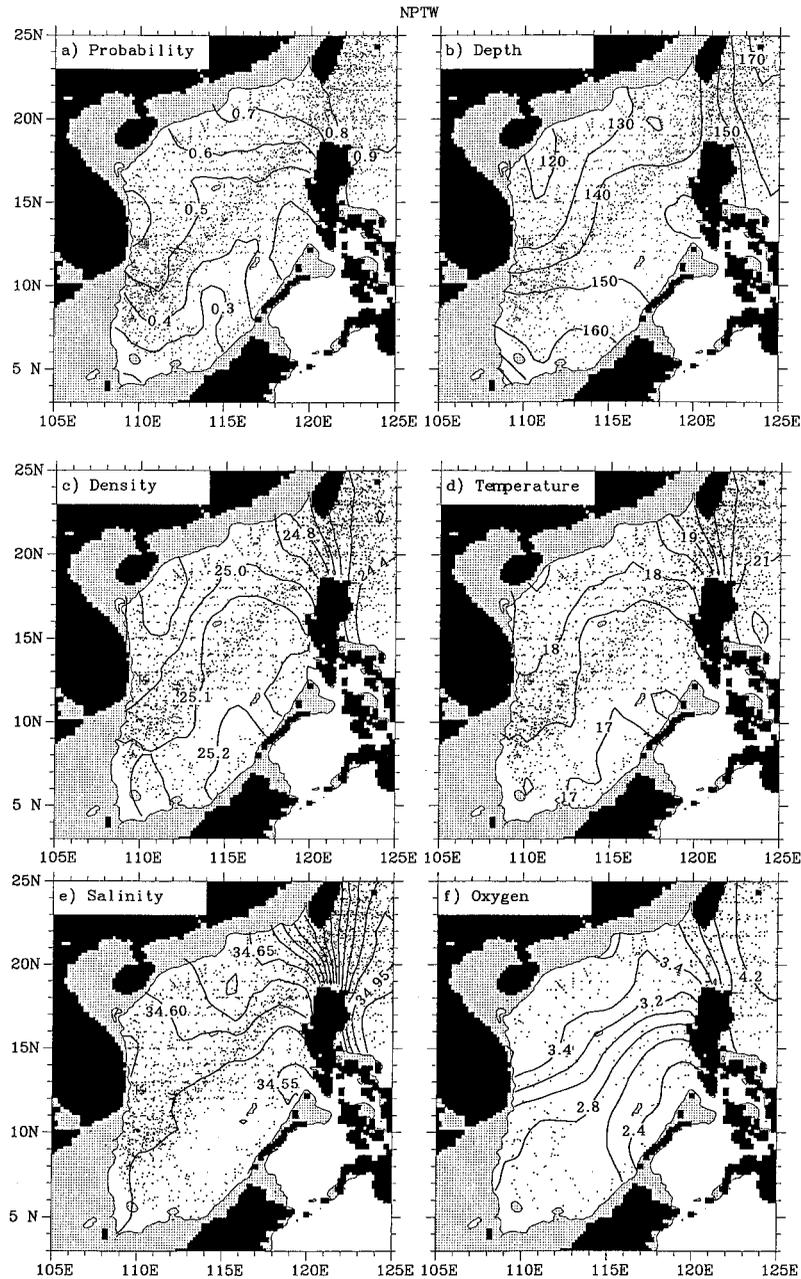
Figure 4. (a) Probability of salinity maximum within the density range of 23.5–25.5 σ_θ, and (b) depth in meters, (c) potential density in kg m^{-3}, (d) potential temperature in °C, (e) salinity in psu, and (f) oxygen concentration in mL L^{-1} in the salinity maximum. Geographic distributions of the stations used to prepare the figures are shown (dots). The region with water depth shallower than 100 m is stippled.

northern tip of Luzon, water has low salinity (<34.58 psu) and is apparently of local origin. Along the continental slope south of China there exists a band of high salinity (>34.60 psu) connecting with the Pacific. Interesting is that the 34.62 isohaline is disconnected around 115°E. Most possibly, this is due to the station distribution in the data, though the isolated pool of high salinity southeast of Hainai could also be explained as the remnant of waters from the previous intrusion. The westward extension of high salinity water occurs as far as 116°E, suggesting that weak intrusion is likely to occur during this period of time.

The high-salinity tongue becomes stronger (>34.68 psu) and extends farther west in summer (June–August, Figure 8b). This pattern is consistent with the earlier speculation that there is a Kuroshio South China Sea branch against the southwest monsoon [cf. *Shaw*, 1989]. The intrusion of high-salinity water from the Kuroshio produces a strong salinity gradient around 15°N, in sharp contrast with the South China Sea water to the south.

The intrusion continues but is slightly weakened from September to November (Figure 8c). Figure 8c has several features in common with those shown in Figures 8a–8b. Most striking is that the location of 34.60 psu isohaline remains rather stable, at between 15° and 18°N, during these three seasons. Previous numerical models [e.g., *Shaw and Chao*, 1994] have suggested that the circulation driven by monsoon in the South China Sea is dominated by an anticyclonic gyre from late spring to early fall. Probably, this anticyclonic circulation
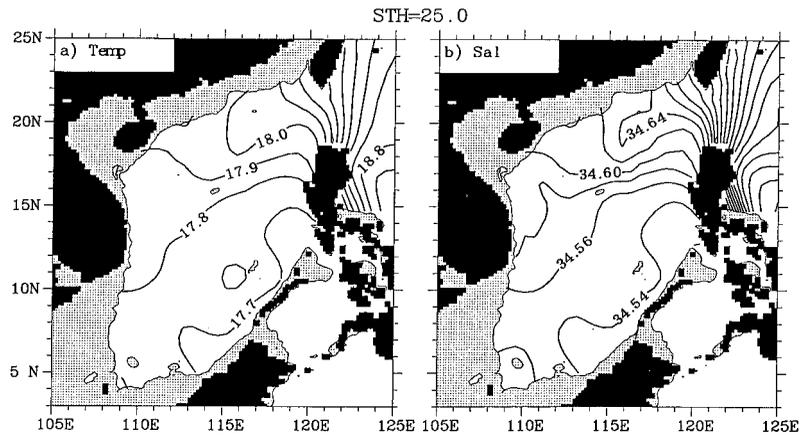
Figure 5. (a) Potential temperature in °C and (b) salinity in psu on 25.0 σ_θ surface.

prevents the high-salinity (>34.60 psu) water from flowing farther south.

The intrusion reaches its maximum strength in winter (December–February), when the northeast monsoon is fully developed (Figure 8d). As part of the cyclonic circulation driven by monsoon, water of high salinity (>34.60 psu) spreads southward to its farthest distance. The distribution of salinity contains a pattern of basically southwest-northeast–oriented contours, with water saltier than 34.60 psu covering the entire basin except for a narrow region northwest of Borneo. Another remarkable feature in Figure 8d is the slight southward shift of the intrusion path from the continental slope south of China to a line primarily between 12°N, 110°E and 20°N, 118°E. We do not know whether this shift is merely an expression of local effects or due to noise in the data at the northwest corner of the basin.

4.2. NPIW

The seasonal distribution in the salinity minimum layer deviates considerably from that aloft. During the transition season of monsoon from March to May, when the intrusion is weakest in the salinity maximum layer, a band of low salinity (<34.40 psu) is seen extending from the Luzon Strait to as far as the coast of Vietnam (Figure 9a). The 34.42 psu isohaline that may be defined as a boundary between the intrusion water and the South China Sea water is roughly located from 10°N, 110°E to 18°N, 120°E. The strong salinity gradient along the coast of Vietnam reflects the sharp contrast of NPIW with local waters.

As southwest monsoon develops, the intrusion starts to decay, and as a result, the 34.42 psu isohaline retreats to the Luzon Strait from June to August (Figure 9b). The lack of intrusion water induces a pattern of homogenous salinity (34.42–34.44) in much of the region studied. There is some indication that a small part of water may escape from the Pacific into the South China Sea along the western coast of Luzon, but it does not appear to make any significant influence on the entire basin.

From September to November the 34.42 psu isohaline continues to shift eastward (Figure 9c). In the meanwhile, relatively high salinity (>34.44 psu) water begins to appear in the central and southern South China Sea. The appearance of the high-salinity core (>34.50 psu) off Borneo and Palawan (also in Figure 7b) is not understood. Isopycnal depth does not show any deeper or shallower distributions that can be related to vertical motion. So this high-salinity core is possibly due to the bad quality of the data amplified by the small number of observations.

Salinity reaches its seasonal maximum in winter, with a high value exceeding 34.44 psu covering the whole basin except for a small region southwest of Taiwan (Figure 9d). Surprisingly, despite the intrusion-favorable northeast monsoon, there is no indication that NPIW enters the South China Sea during this season. Instead, a high-salinity tongue is seen extending from the coast of Vietnam to the Luzon Strait. *Chao et al.* [1996a] suggested that there is a deep upwelling induced by orographic lifting of currents over the continental margin off Vietnam from August to December. Figure 9d seems to support their speculation. Because of this deep upwelling, salt water may be sucked from below and carried offshore in the salinity minimum layer.

5. Circulation

The circulation in the South China Sea was first described by *Wyrtki* [1961], based on earlier hydrographic observations, sea level records, and ship drifts, and later simulated by several basin-scale models [e.g., *Shaw and Chao*, 1994]. According to these earlier studies the circulation in the South China Sea is chiefly forced by monsoon, cyclonic in winter and anticyclonic in summer, and as a result eastward and westward flows occur in the Luzon Strait alternately during the year. Recent studies [*Metzger and Hurlburt*, 1996; *Qu*, 1999] further suggest that the annual mean transport through the Luzon Strait is not negligible and may have a notable impact on the South China Sea circulation.

Figure 10 shows the geostrophic flow at 100 m computed from the dynamic height distribution (relative to 400 db) prepared by *Qu* [1999, Figure 4]; using historical temperature profiles combined with the climatological *T/S* relationship. The agreement between Figures 8 and 10 is generally good. Despite considerable variability a westward flow can be seen during all seasons of the year following the intrusion path of the North Pacific waters. From late spring through early fall (Figures 10a–10c) this westward flow is narrowly confined in the continental slope south of China and does not appear to follow the western boundary throughout. Immediately to the south is an opposite directed current, which is supposed to be related to the anticyclonic gyre suggested by *Wyrtki* [1961] during that period of time. As the basin-scale cyclonic gyre develops in winter (Figure 10d), the westward flow is present in a broad region south of China and allows the intrusion water to spread in the entire basin of the South China Sea (Figure 8).

Another important result inferred from the property distribution is that waters in the salinity maximum and minimum
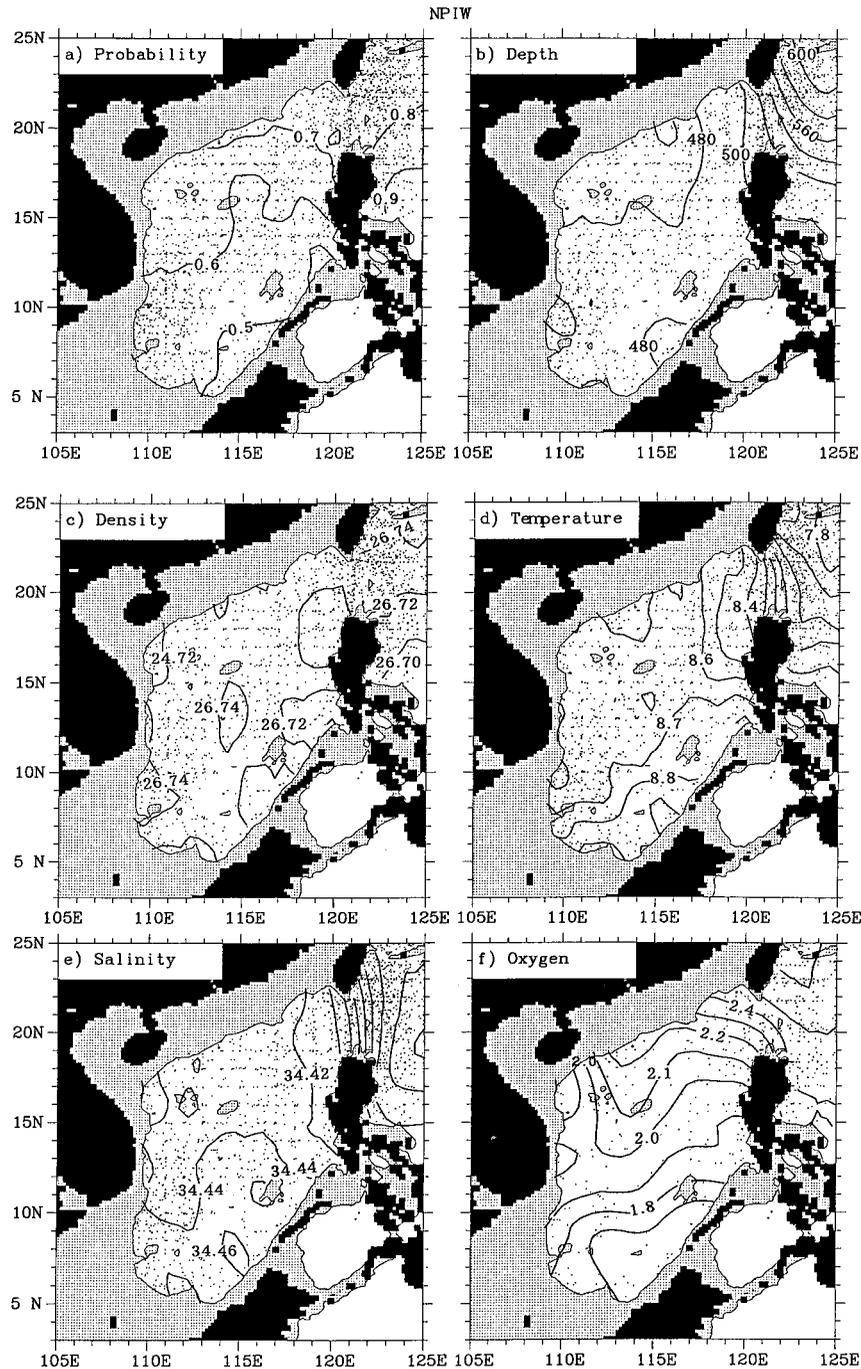
NPIW

Figure 6. Same as Figure 4 except for the salinity minimum within the density range of 26.5–27.0 σ_θ. The region with water depth shallower than 500 m is stippled.

layers flow in the opposite direction [see also *Wyrtki*, 1961]. The reference level chosen in preparing Figure 10 is apparently too shallow to resolve this structure. However, the two-layer circulation pattern has been successfully reproduced in general circulation models (S. K. Behera, personal communication, 1999). Further investigation of the model results is under way.

6. Mechanism of the Intrusion

Several hypotheses have been raised concerning the mechanism of the intrusion. Based on a series of numerical experiments, *Metzger and Hurlburt* [1996] suggested that the mean Luzon Strait

transport is mainly a function of the large-scale forcing of the Pacific and the model geometry in the Sulu Sea. In fact, their results can be explained by the "island rule" put forward by *Godfrey* [1989] and later modified by *Wajsowicz* [1993]. Careful examination of the bathymetric charts shows that there is a narrow passage (Sibutu strait) in the Sulu Sea connecting the South China Sea with the Pacific Ocean (Figure 1). Although this passage is only about 1/8° wide at the 200-m isobath and has a sill depth of about 250 m, it makes the Philippines a completely isolated island in the Pacific. By mass continuity the Luzon Strait transport should be quite accurately given by
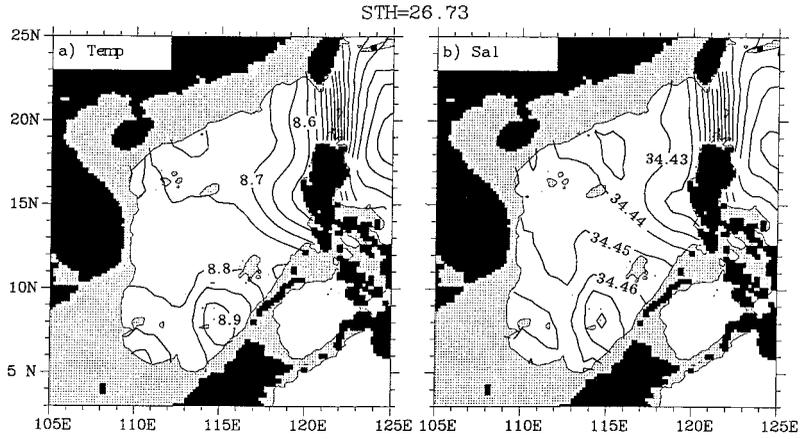
STH=26.73

Figure 7. (a) Potential temperature in °C and (b) salinity in psu on 26.73 σ_θ surface.

$$T_l = T_0 + T_t - T_b, \tag{1}$$

where T_l represents the Luzon Strait transport, T_t is the Taiwan Strait transport, T_b is the Bering Strait transport, and T_0 is the total transport across the Pacific at the southern tip of Mindanao. T_t and T_b have been studied by earlier studies, being of the order of 2.0 and 0.8 Sv (1 Sv = 10^6 m^3 s^{-1}), respectively, in the mean [*Fang et al.*, 1991; *Coachman and Aagaard*, 1988]. So for the zero-order approximation, we have $T_l = T_0 + 1.2$.

According to the "island rule" [*Godfrey*, 1989], T_0 can be calculated explicitly from the integral of the long-path component of wind stress along the closed path ABCD; that is,

$$T_0 = \frac{1}{(f_D - f_A)} \oint_{ABCD} \frac{\tau^{(l)}\, dl}{\rho_0}, \tag{2}$$

where $\tau^{(l)}$ denotes the long-path component of wind stress, A is at the southern tip of Mindanao, and D is at the northern tip of Luzon (Figure 1). B and C represent the two points at the same latitudes as A and D at the American coast; f_A, f_D are the Coriolis parameters at A and D, respectively. The inte-
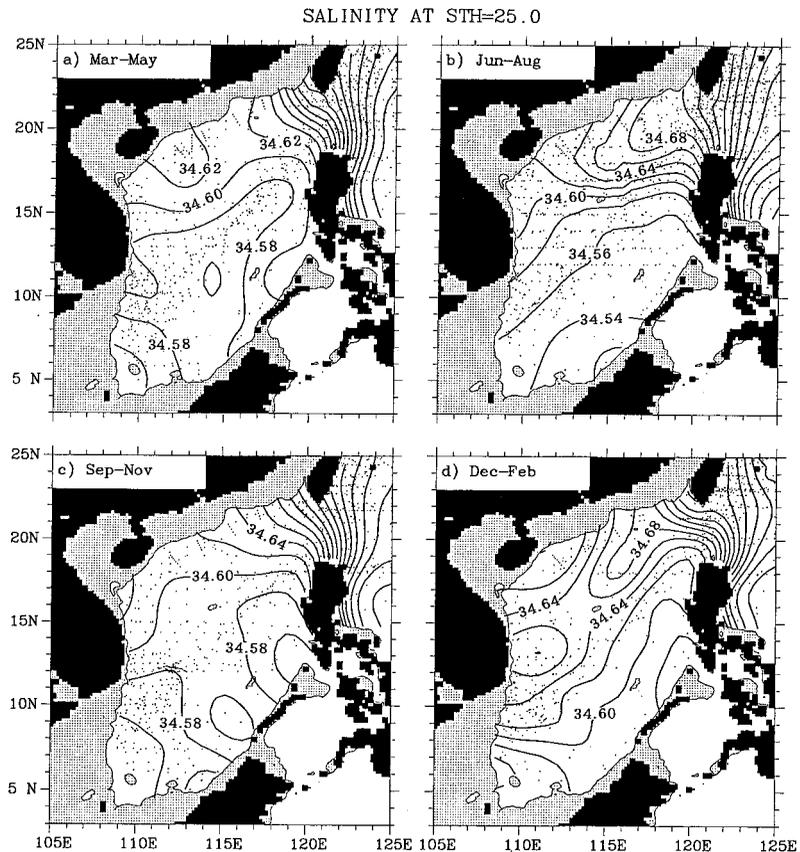
SALINITY AT STH=25.0

Figure 8. Seasonal variation of salinity (psu) on 25.0 σ_θ surface.
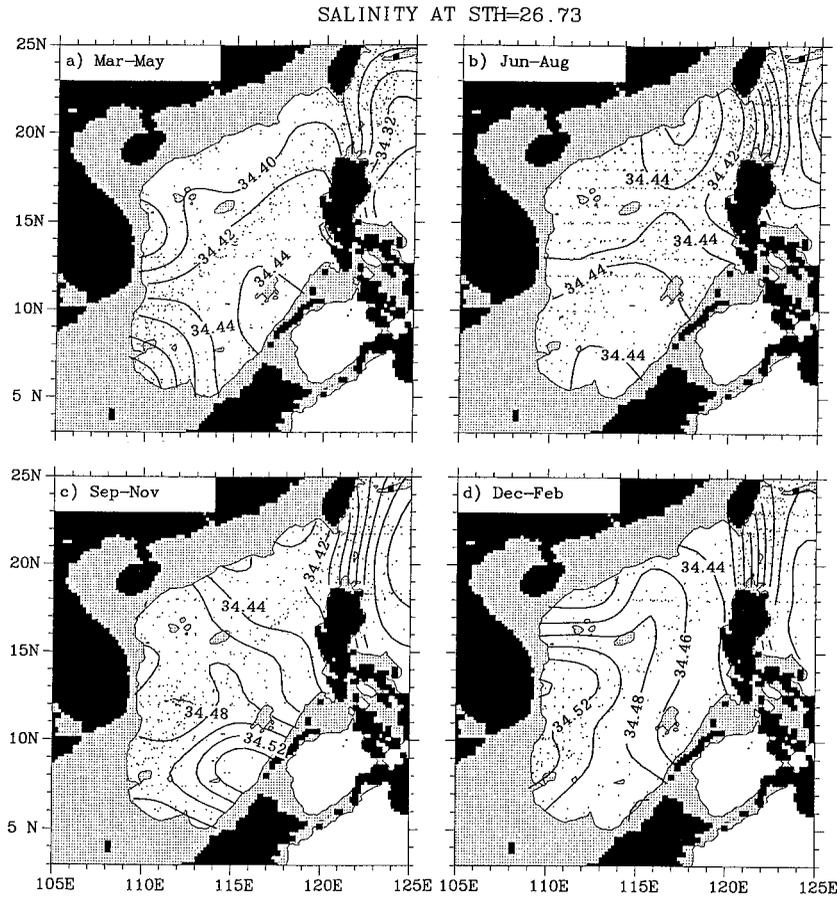
SALINITY AT STH=26.73

Figure 9. Seasonal variation of salinity (psu) on 26.73 σ_θ surface.

gral taken from D to A is along the western coast of the Philippines.

In deriving (2) an important assumption made is that the Philippines does not penetrate the oceanic western boundary layer in the Sulu Sea, and thus friction along the western coast of the Philippines can be neglected. The presence of the narrow and shallow passages in the Sulu Sea breaks down this assumption, so an extra term representing the frictional effect F must be added to (2), leading to the modified "island rule" [*Wajsowicz*, 1993, equations (4.1) and (4.6)]:

$$T_0 = \frac{1}{(f_D - f_A)} \oint_{ABCD} \frac{\tau^{(l)}\, dl}{\rho_0} + \frac{1}{(f_D - f_A)} \int_{DA} F\, dl. \quad (3)$$

In (3) the integral of wind stress from D to A is at least an order smaller than for the path ABCD [*Hellerman and Rosenstein*, 1983], so the mean transport through the Luzon Strait can be reasonably explained as a result of counterbalance between the large-scale forcing of the Pacific and the frictional effect along the western coast of the Philippines.

The first term in (3) is estimated to be 16 Sv from Hellerman and Rosenstein's annual mean wind stress. This value is apparently much larger than one would expect from the property distribution (sections 3 and 4) and therefore must be reduced considerably by frictional effect. For the equilibrium response to a steady wind stress, the frictional effect can be estimated from measurements of the depth-integrated dynamic height difference between the north and the south sides of the Sulu

Archipelago [*Wajsowicz*, 1993], namely, between E and F (Figure 1). We found little change in depth-integrated dynamic height along the western coast of Luzon, based on the *Levitus* [1982] climatology of temperature and salinity. Hence

$$\frac{1}{(f_D - f_A)} \int_{DA} F\, dl = \frac{-1}{(f_D - f_A)} \int_{DA} \tau^{(l)}\, dl + \frac{g}{(f_D - f_A)} \Delta P_{EF}. \tag{4}$$

The depth-integrated dynamic height, relative to 1000 db, drops by about 45 m² from E to F. In the annual mean the longshore wind stress is generally weak in the region, and so from (4), the reduction in the Luzon Strait transport due to frictional effect is $(g/(f_D - f_A))\Delta P_{EF} \sim 13$ Sv, which accounts for about 80% of the value (16 Sv) achievable for a wide channel without frictional effect. This yields an estimate of $T_0 \sim 3$ Sv, or equivalently, $T_l \sim 4.2$ Sv in the mean, comparable with that from geostrophic calculation of the upper 400 m [*Qu*, 1999].

The application of the "island rule" provides the theoretical basis for understanding the intrusion dynamics in the Luzon Strait. It also explains why the Luzon Strait transport is especially sensitive to the model geometry, namely whether the Sibutu strait in the Sulu Sea is open or closed [*Metzger and Hurlburt*, 1996]. If this passage were closed in the model, the South China Sea would simply become a semiclosed marginal sea, except for several very shallow (<30 m) straits on the Sunda shelf. In this case, there would be no circulation around the Philippines, and as a result, the Luzon Strait transport
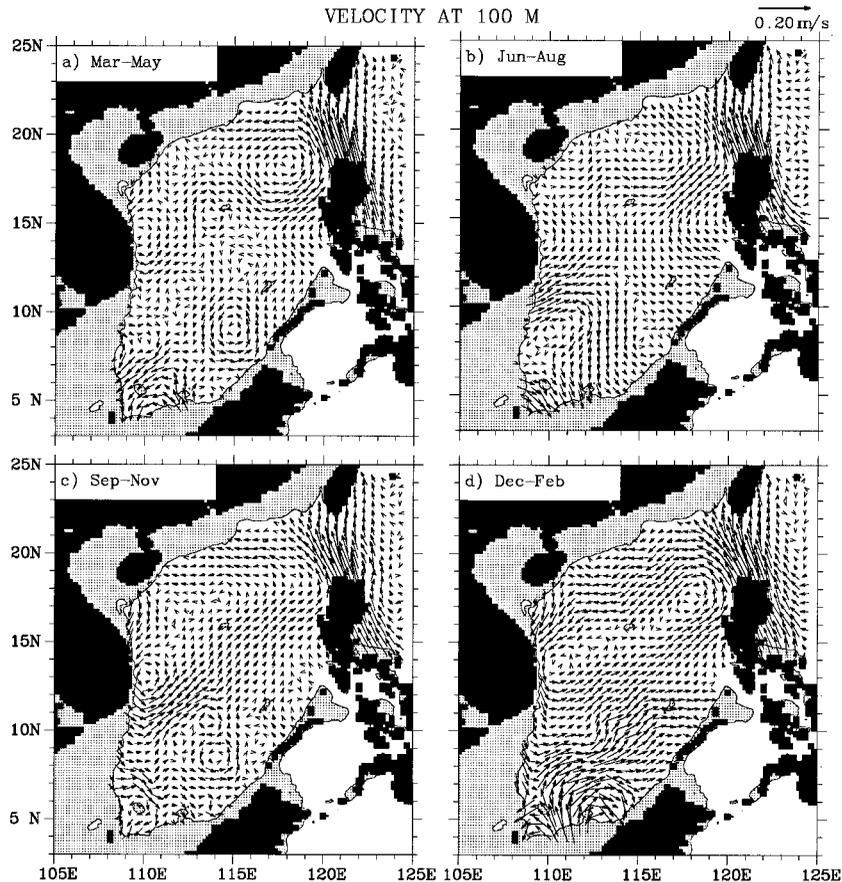
Figure 10. Seasonal variation of geostrophic velocity (m s^{-1}) at 100 m relative to 400 db.

would be precisely equal to the Taiwan Strait transport and of the order of 2 Sv in the mean. On the other hand, if this passage were too wide and deep in the model, the frictional effect would be reduced, thus leading to an overestimate of the Luzon Strait transport.

It is important to note that the "island rule" is valid only for timescales greater than the baroclinic Rossby adjustment timescale in a variable bottomed ocean [*Wajsowicz*, 1993]. As the time taken for a baroclinic Rossby wave to cross the Pacific and back along the path ABCD is more than a year, this simple theory is not expected to be applicable to the seasonal cycle. Results from numerical models [e.g., *Metzger and Hurlburt*, 1996; *Chao et al.*, 1996b] have suggested that the monsoonal wind is an important mechanism inducing the seasonal variation of the intrusion by strengthening the sea level along the south China coast in winter and weakening it in summer. The details should be investigated further by research.

7. Summary and Discussion

This study shows evidence that waters of both the salinity maximum and the salinity minimum exist in the South China Sea. Despite considerable modification of characteristics because of mixing, these waters can be traced to as far south as the coast of Borneo along density surfaces of 25.0 and 26.73 σ_θ, respectively. Consonant with several earlier observations [e.g., *Wyrtki*, 1961; *Nitani*, 1972], we found strong property gradients in the Luzon Strait. Mixing of temperature and salinity alters the density of NPTW by about 0.5 kg m^{-3} with the higher value

on the South China Sea side, while the density of NPIW remains rather stable as it crosses the Luzon Strait. On the average, the depth of NPTW and NPIW is 50–100 m shallower in the South China Sea than in the Philippine Sea. This could be either due to the presence of the western Pacific warm pool water on the eastern side of the Luzon Strait or due to deep upwelling in the South China Sea [*Nitani*, 1972; *Chao et al.*, 1996a].

In the salinity maximum layer, water property distribution suggests an intrusion from the Pacific into the South China Sea all year-round through the Luzon Strait, and this seems to be consistent with the picture of circulation prepared by *Qu* [1999]. From spring to fall the intrusion water is narrowly confined in the continental margin south of China; only in winter, when northeast monsoon is developed, can it spread in the southern South China Sea. This reflects the strong influence of monsoon on the seasonal variation of the intrusion, although it has little effect in the mean.

Interesting is that the intrusion in the salinity maximum layer has greater strength in summer than prior to and after it, despite the prevailing southwest monsoon. *Qu* [1999] has examined the longshore pressure gradient along the continental slope south of China and demonstrated exactly the same phase as the intrusion strength described above, with maxima in winter and summer and minima in spring and fall. This led him to suggest that the intrusion of waters from the Pacific into the South China Sea is primarily driven by the longshore pressure gradient.

Water of salinity minimum (NPIW) also enters through the Luzon Strait and spreads in the South China Sea, but its sea-

sonal variation is completely out of phase with that of salinity maximum (NPTW). NPIW leaks into the South China Sea only in spring, when the intrusion of NPTW is weakest. This lends support to the previous speculation that the two water masses move in the opposite direction [*Wyrtki*, 1961].

A dynamical consideration of the intrusion by applying the "island rule" to the Philippines suggests that the intrusion is a result of counterbalance between the large-scale forcing of the Pacific and the friction created in the Sulu Archipelago. A combined use of the "island rule" with climatological data yield a transport estimate of about 4.2 Sv. For future modeling studies, this result implies that to get a reasonable estimate of the intrusion, the domain of the numerical model would have to extend southward to the southern tip of the Philippines and eastward to the western coast of America. The spatial resolution of the model would also have to be fine enough to resolve most of the narrow passages that connect the South China Sea with the Pacific and Indian Oceans, typically of 10 km wide and 100 m deep.

Appendix

Standard deviations (STDs) of properties were obtained during the averaging process, based on ensembles of 5–20 stations at each grid. The spatial distributions of STDs, though not presented here, are generally uniform in much of the region studied. The STD of potential temperature is large, reaching the order of 1°C in the salinity maximum layer within the depth range of the seasonal thermocline; this value decreases with depth to about 0.5°C in the salinity minimum layer. The STD of salinity is relatively stable, with the typical value defined as the average over the domain studied not exceeding 0.05 psu both in the salinity maximum and in the salinity minimum layers. Accordingly, the typical STD of potential density (as a function of potential temperature and salinity) reaches 0.28 and 0.1 kg m^{-3}, respectively, in the two layers. When water masses are traced using isopycnal surfaces, the STD of potential temperature is reduced (<0.25°C), but the STD of salinity remains almost the same. The STDs of the depth and oxygen concentration in the salinity extremes are also estimated, in reasonable agreement with those discussed for potential temperature and salinity.

The impression one would obtain from the error analysis is that time variability is fairly large, being of comparable if not greater strength with the mean fields, indicative of strong eddy activities in the South China Sea. However, it must be noted that the large STDs could also be due to the bad quality of the data. Because most of the observations were made at conventional standard depths, the determination of the salinity extremes is subject to a large uncertainty, in particular with regard to the salinity minimum of which the vertical separation of sampling is typically 100 m. The effect of this uncertainty could be reduced by the combined use of data from various cruises in different seasons of different years.

Although there is no easy way to quantify how complete the mean fields are in a statistical sense, most of the large-scale (>300 km) phenomena shown above seem to be insensitive to the methods of analysis and the presentation of the data. Thus our conclusions regarding the intrusion and its seasonal variation should be robust. They are unlikely to be modified in a qualitative sense, though quantitative differences are probable.

References

Chao, S. -Y., P. -T. Shaw, and S. Y. Wu, Deep sea ventilation in the South China Sea, *Deep Sea Res., Part I*, *43*, 445–466, 1996a.

Chao, S. -Y., P. -T. Shaw, and S. Y. Wu, El Nino modulation of the South China Sea circulation, *Prog. Oceanogr.*, *38*, 51–93, 1996b.

Coachman, L. K., and K. Aagaard, Transports through Bering Strait: Annual and interannual variability, *J. Geophys. Res.*, *93*, 15,535–15,539, 1998.

Fang, G., B. Zhao, and Y. Zhu, Water volume transport through the Taiwan strait and the continental shelf of the East China Sea measured with current meters, in *Oceanography of Asian Marginal Seas, Elsevier Oceanogr. Ser.* vol.54, edited by K. Takano, pp. 345–358, Elsevier Sci. New York, 1991.

Godfrey, J. S., A Sverdrup model of the depth-integrated flow for the world ocean allowing for island circulations, *Geophys. Astrophys. Fluid Dyn.*, *45*, 89–112, 1989.

Hellerman, S., and M. Rosenstein, Normal monthly wind stress over the world ocean with error estimates, *J. Phys. Oceanogr.*, *13*, 1093–1104, 1983.

Levitus, S., Climatological atlas of the world oceans, *NOAA Prof. Pap.*, *13*, U.S. Govt. Print. Off., Washington, D.C., 1982.

Lukas, R., E. Firing, P. Hacker, P. L. Richardson, C. A. Collins, R. Fine, and R. Gammon, Observations of the Mindanao current during the western equatorial Pacific Ocean circulation study, *J. Geophys. Res.*, *96*, 7089–7104, 1991.

Metzger, E. J., and H. E. Hurlbert, Coupled dynamics of the South China Sea, the Sulu Sea, and the Pacific Ocean, *J. Geophys. Res.*, *101*, 12,331–12,352, 1996.

Nitani, H., Beginning of the Kuroshio, in *Kuroshio: Its Physical Aspects of the Japan Current*, edited by H. Stommel and K. Yoshida, pp. 129–163, Univ. of Wash. Press, Seattle, 1972.

Qu, T., Upper layer circulation in the South China Sea, *J. Phys. Oceanogr.*, in press, 1999.

Qu, T., H. Mitsudera, and T. Yamagata, on the western boundary currents in the Philippine Sea, *J. Geophys. Res.*, *103*, 7537–7548, 1998.

Qu, T., H. Mitsudera, and T. Yamagata, A climatology of the circulation and water mass distribution near the Philippine coast, *J. Phys. Oceanogr.*, *29*, 1488–1505, 1999.

Reid, J. L., Intermediate waters of the Pacific Ocean, *Johns Hopkins Oceanogr. Study*, *2*, 1–85, 1965.

Shaw, P. -T., The intrusion of water masses into the sea southwest of Taiwan, *J. Geophys. Res.*, *94*, 18,213–18,226, 1989.

Shaw, P. -T., Seasonal variation of the intrusion of the Philippine seawater into the South China Sea, *J. Geophys. Res.*, *96*, 821–827, 1991.

Shaw, P. -T., and S. -Y. Chao, Surface circulation in the South China Sea, *Deep Sea Res., Part I*, *41*, 1663–1683, 1994.

Tsuchiya, M., Upper waters of the intertropical Pacific Ocean, *Johns Hopkins Oceanogr. Study*, *4*, 1–50, 1968.

Wajsowicz, R. C., The circulation of the depth-integrated flow around an island with application to the Indonesian throughflow, *J. Phys. Oceanogr.*, *23*, 1470–1484, 1993.

Wyrtki, K., Physical oceanography of the southeast asian waters, *Naga Rep. 2*, 195 pp., Scripps Inst. of Oceanogr., La Jolla, Calif., 1961.

H. Mitusdera, Frontier Research System for Global Change, Tokyo International Pacific Research Center, SOEST, University of Hawaii, Honolulu, HI 96822.

T. Qu, International Pacific Research Center, SOEST, University of Hawaii, 2525 Correa Road, Honolulu, HI 96822.

T. Yamagata, Department of Earth and Planetary Physics, University of Tokyo, Tokyo Frontier Research System for Global Change, Tokyo, Japan.